Lithography simulation employing rigorous solutions to Maxwell's equations

Ron Gordon, Chris A. Mack
FINLE Technologies, Inc.
PO Box 162712, Austin, TX 78716
Email: Ron_Gordon@finle.com

Abstract

A method of obtaining rigorous solutions to Maxwell's equations for the transmission of light through a photomask, both chrome-based and phase-shifting, is presented. The electromagnetic simulator will predict the transmission of light through the mask taking into account material properties, width, and thickness of the structures on the mask. This electromagnetic simulation will then be incorporated into the software package PROLITH/2 for complete simulation down to the resist level. Examples of lithography simulation using these rigorous solutions will be presented.

Keywords: Maxwell's equations, Kirchhoff approximation, lithography simulation, absorbing boundary conditions.

1. Introduction

1.1. Need for simulation

Lithography simulation, including the calculation of the projected image of a photomask pattern onto a resist coated wafer, has become an indispensable tool for lithography research, development and manufacturing. Much work recently has centered on the improvement of the accuracy of these models for smaller features at higher numerical apertures. In particular, vector treatment of the electromagnetic field propagating through the resist is now common. However, typical reduction factors of 4 - 5X mean that mask features are relatively large compared to the wavelength of the imaging light. As a result, the use of scalar approximations on the mask side of the imaging problem are quite common. In other words, when the smallest feature size on the mask is much larger than λ, the Kirchhoff approximation, which treats the mask as a thin plane with geometric transmission, provides sufficient accuracy. When this is not the case, it becomes essential that the material composition and actual physical dimensions of the mask are taken in to account via a rigorous solution to Maxwell's equations.

In PROLITH/2, the electric field distribution in the neighborhood of the wafer plane, defocused by a distance y, is computed via the following (scalar) expression[1]:

$$E(x,y) = \int_{-\infty}^{\infty} df_x \, M(f_x) P(f_x) \exp\left[i2\pi\left(f_x x + f_y y\right)\right] \tag{1.1}$$

where

 0277-786X/98/$10.00

Downloaded From: http://proceedings.spiedigitallibrary.org/ on 06/02/2014 Terms of Use: http://spiedl.org/terms

$$f_y \equiv \begin{cases} \sqrt{1/\lambda^2 - f_x^2}, & |f_x| \le 1/\lambda, \\ +i\sqrt{f_x^2 - 1/\lambda^2}, & |f_x| > 1/\lambda, \end{cases} \tag{1.2}$$

$$M(f_x) = \int_{-\infty}^{\infty} dx'\, E(x', 0^+) \exp(-i2\pi f_x x'), \tag{1.3}$$

λ is the vacuum wavelength of the (monochromatic) radiation, $E(x', 0^+)$ is the field just below the mask, f_x is the spatial frequency coordinate in the pupil plane, and $P(f_x)$ represents the pupil function of the lens and contains all the information about the finite size of the exit pupil and all possible wavefront aberrations in the objective. The quantity y in Eq. (1.1) is the amount of defocus when the coordinate system is centered at the geometrical focus (assumed to lie on the optical axis) because, in optical lithography, the objective lens is assumed to be image-side telecentric (i.e., its exit pupil is at infinity). Also note that the branch of the square root in Eq. (1.2) is chosen so that this electric field satisfies radiation boundary conditions at infinity; that is, there is no inward-propagating field coming from outside the optical system.

Within the assumptions just outlined, and assuming the light incident on the mask is unpolarized, the field expression in Eq. (1.1) is exact in that it satisfies the wave equation, as long as the value of the field just behind the mask, $E(x', 0^+)$, is chosen correctly. The most natural assumption to make is that the field in that plane simply takes the value

$$E(x', 0^+) \approx m(x'). \tag{1.4}$$

where $m(x')$ is the ideal amplitude transmittance of the mask. Eq. (1.4) is a form of the Kirchhoff approximation[2]. It is well known[3] that, when the smallest feature on the mask $D_{\min}$ and the distance between the plane of observation and the mask are larger than λ, Eq. (1.4) provides an accurate estimate of the field to within an error of the order of $\lambda / D_{\min}$. Furthermore, Eq. (1.1) is easily computed, as all integrals are simply Fourier transform relations.

There are cases in optical lithography, however, where the size of the smallest feature of the mask is of the order of λ; in such instances, Eq. (1.4) is no longer accurate. This can be found, for example, in phase-shifting masks, optical-proximity correcting masks, and 1:1 projection lithography. The initial field $E(x', 0^+)$ must then be determined through the rigorous boundary conditions from Maxwell's equations. For the general planar structures that make up the masks of interest in projection lithography, an exact analytical expression for this initial field distribution is out of the question. Therefore, an efficient, robust numerical method is necessary to find this field and, ultimately, to decide precisely at what point the Kirchhoff approximation becomes unacceptable.

1.2. Goals of this paper

Much research in determining the effects of mask topography on the aerial image has been carried out in recent years[4,5,6,7,8]. The goal of this paper is twofold: to find examples where the Kirchhoff approximation is no longer valid and to analyze the effects of mask topography within the PROLITH™ simulation environment. The examples to be considered here will take their cues from optical proximity correction and phase-shifting masks. In Section 2, a brief review of the governing equations and boundary conditions is presented. An outline of the

Downloaded From: http://proceedings.spiedigitallibrary.org/ on 06/02/2014 Terms of Use: http://spiedl.org/terms

numerical technique we chose to implement for the solution to these equations, the finite-difference time-domain method, is also given. A comparison with the exact solution of the perfectly conducting half-plane will provide a preliminary evaluation of this algorithm. The main result of these computations is a modified transmittance function for the mask. The transmittance function is then integrated into PROLITH/2, and this is discussed in Section 3. Comparison with the Kirchhoff approximation is discussed in Section 4 through several examples taken from typical masks.

2. Theory

2.1. Maxwell's equations

The vector nature of the electromagnetic field is defined by Maxwell's equations, and these equations are written as follows (in MKS units):

$$\nabla \times \mathbf{E} + \frac{\partial}{\partial t}\mathbf{B} = \mathbf{0}, \tag{2.1}$$

$$\nabla \times \mathbf{H} - \frac{\partial}{\partial t}\mathbf{D} = \mathbf{J}, \tag{2.2}$$

and, for the linear, isotropic media considered here, the following equations are satisfied:

$$\mathbf{D} = \varepsilon \mathbf{E}, \tag{2.3}$$

$$\mathbf{B} = \mu \mathbf{H}, \tag{2.4}$$

$$\mathbf{J} = \sigma \mathbf{E}. \tag{2.5}$$

Here, ε is the permittivity, μ is the permeability, and σ is the conductivity of the material in which the electromagnetic disturbance is taking place. [The complex index of refraction for a time-harmonic disturbance is then given by[9] $n^2 = \varepsilon\mu / \varepsilon_0\mu_0 + i\sigma\mu\lambda / \left(2\pi\sqrt{\varepsilon_0\mu_0}\right)$, where λ is the wavelength of the disturbance.] In this paper, only the fields **E** and **H** are of concern. For wave propagation in the general, isotropic case, there are then 6 coupled equations to consider. Also note that, in the absence of any sources, both the electric and magnetic fields **E** and **H** satisfy the vector wave equation independently.

A major simplification is possible when one can neglect the variation of the fields in one of the transverse directions [the $\hat{z}$ direction in this paper]. In this case, it turns out that a disturbance with an arbitrary polarization – which, in general, is represented by a set of 6 scalar fields - can be expressed as a linear combination of 2 sets of 3 scalar fields[10]. Each of these sets has an orthogonal polarization with respect to the other basis. The equations satisfied by the fields in these bases, taking into account the linearity of the media expressed in Eqs. (2.3), (2.4) and (2.5) are as follows:

E-polarization: $\left(H_x, H_y, E_z\right)$

$$\mu \frac{\partial}{\partial t} H_x = -\frac{\partial}{\partial y} E_z, \tag{2.6}$$

Downloaded From: http://proceedings.spiedigitallibrary.org/ on 06/02/2014 Terms of Use: http://spiedl.org/terms

$$\mu \frac{\partial}{\partial t} H_y = \frac{\partial}{\partial x} E_z , \tag{2.7}$$

$$\varepsilon \frac{\partial}{\partial t} E_z + \sigma E_z = \frac{\partial}{\partial x} H_y - \frac{\partial}{\partial y} H_x . \tag{2.8}$$

H-polarization: $\left(E_x, E_y, H_z\right)$

$$\varepsilon \frac{\partial}{\partial t} E_x + \sigma E_x = \frac{\partial}{\partial y} H_z , \tag{2.9}$$

$$\varepsilon \frac{\partial}{\partial t} E_y + \sigma E_y = \frac{\partial}{\partial x} H_z , \tag{2.10}$$

$$\mu \frac{\partial}{\partial t} H_z = \frac{\partial}{\partial y} E_x - \frac{\partial}{\partial x} E_y . \tag{2.11}$$

Note that E-polarization implies that the electric field has only a z-component, while all others are zero, and similarly for H-polarization. To find the scattered field for an arbitrarily polarized incident field, one simply decomposes the polarization into the above basis. The fields in each basis set can then be found separately for any scattering problem. For the remainder of this paper, only E-polarization will be considered.

Note that, for most materials of interest in lithography, $\mu = \mu_0$ and it will be assumed that this is true throughout the paper. Therefore, given a complex index of refraction, we can uniquely find the relative permittivity and the conductivity without any additional information.

2.2. Boundary Conditions

2.2.1. At a discontinuity

Of interest is the behavior of the field in the neighborhood of an interface. By analyzing Maxwell's equations in a small region about the discontinuity surface, one can deduce the following relations between the fields on either side of the interface of interest:

$$[\hat{\mathbf{y}} \times \mathbf{E}]_+ - [\hat{\mathbf{y}} \times \mathbf{E}]_- = \mathbf{0}, \tag{2.12}$$

$$[\hat{\mathbf{y}} \times \mathbf{H}]_+ - [\hat{\mathbf{y}} \times \mathbf{H}]_- = \mathbf{J}, \tag{2.13}$$

where the $\hat{y}$ direction points from the "-" to the "+" side of the interface, and J represents the surface current density at the interface. For E-polarization, Eqs. (2.12) and (2.13) are conditions for E_z and H_x, while they are conditions for E_x and H_z for H-polarization. Thus, the tangential component of the electric field is continuous at an interface, while that for the magnetic field is discontinuous.

Note that Eqs. (2.6) - (2.11) allow for the special case of a perfectly conducting material. Such a case corresponds to having $\sigma = \infty$, and, by the continuity of the tangential electric field $E_{\tan}$, Eqs. (2.8) and (2.9) would imply that $E_{\tan} = 0$, as expected from Eq. (2.12). [Note that the normal component of the electric field in Eq. (2.10) does not satisfy this relation because it is not continuous across the discontinuity.] This case will prove of

Downloaded From: http://proceedings.spiedigitallibrary.org/ on 06/02/2014 Terms of Use: http://spiedl.org/terms

great importance in verifying that the numerical routine used here is correct, as one of the few known rigorous analytical solutions to the problem of electromagnetic diffraction by an aperture requires an infinitely thin, perfectly conducting screen.

In all other cases, an exact analytical solution is presently beyond our means. Since the quantities in Eqs. (2.12) and (2.13) are unknown in general, the boundary conditions become extremely difficult to implement. There has been much literature written about using tractable approximations to these boundary conditions in special cases to find closed-form approximations to the scattered fields [11]. Although such approximations may prove useful in crosschecking the solutions obtained from numerical methods, their discussion is beyond the scope of this paper.

2.2.2. At Infinity

As mentioned in the Introduction, the behavior of the electric field far from the media must be specified in order to be guaranteed a unique field everywhere in the domain of interest. The behavior sought in radiation problems is that the field in the far zone must ultimately behave as a pure outgoing wave uniformly over angle [12]. It has been shown that such a requirement in the 2D case leads to an asymptotic expansion for each scattered field component $E^{(s)}(\mathrm{r})$ [defined to be the total field minus the incident field] of the form[13]

$$E^{(s)}(\mathrm{r}) \sim H_0^{(1)}(kr)\sum_{n=0}^{\infty} r^{-n} F_n(\theta) + H_1^{(1)}(kr)\sum_{n=1}^{\infty} r^{-n} G_n(\theta). \tag{2.14}$$

In principle, one could use this "pseudo-boundary condition" to find a unique, or asymptotic, expression for the electromagnetic field due to a scattering object. Because of the intractable form of the boundary conditions, however, a numerical scheme is sought here, and a more general treatment of these far-zone conditions is to be employed. Before such conditions are discussed, the numerics must first be mapped out.

2.3. The Finite-Difference Time-Domain Method

The numerical method of choice here is known as the Finite-Difference Time-Domain (FDTD) method. It turns out that this method is ideally suited to the rectangular geometries that are natural in mask topography. The principle is simple: replace the time and space derivatives in Maxwell's equations by their discrete analogs and update the equations in time. On the other hand, the choices of discrete analogs (e.g., forward difference, backward difference, etc.) and spatial and temporal sampling is crucial in determining stability, run time, and storage.

The sampling scheme used here follows a grid of so called "Yee cells"[14], which is simply the result of using a centered-differencing scheme for both the spatial and temporal derivatives. The immediate advantage of centered-differencing is in its order doubling: if the sampling distance is a small number h, then while the error in using forward- or backward-differences is $O(h)$, that for using centered-differencing is $O(h^2)$. More importantly, and less obviously, is the fact that forward-differencing is unconditionally unstable, while centered-differencing is stable, subject to the Courant condition[15]:

$$\frac{1}{\Delta\tau^2} \geq \frac{1}{\Delta x^2} + \frac{1}{\Delta y^2}, \tag{2.15}$$

Downloaded From: http://proceedings.spiedigitallibrary.org/ on 06/02/2014 Terms of Use: http://spiedl.org/terms

where $\tau = ct$, c is the vacuum speed of light, $\Delta\tau$ is the distance light travels in one time step, and Δx and Δy represent the cell spacings in the numerical grid. Such centered differencing leads to a pattern of interwoven electric and magnetic field values on a computational grid.

Let the grid dimensions be $[-X, X]\times[-Y, Y]$, and let $x = -X + j\Delta x$, $y = Y - k\Delta y$, and $\tau = n\Delta\tau$. Eqs. (2.6) to (2.8) then take the discrete form:

$$H_x(j,k+1/2,n+1/2) = H_x(j,k+1/2,n-1/2) - \sqrt{\frac{\varepsilon_0}{\mu_0}}\frac{\Delta\tau}{\Delta y}\left[E_z(j,k+1,n) - E_z(j,k,n)\right], \tag{2.16}$$

$$H_y(j+1/2,k,n+1/2) = H_y(j+1/2,k,n-1/2) + \sqrt{\frac{\varepsilon_0}{\mu_0}}\frac{\Delta\tau}{\Delta x}\left[E_z(j+1,k,n) - E_z(j,k,n)\right], \tag{2.17}$$

$$\begin{aligned} E_z(j,k,n+1) &= \beta E_z(j,k,n) \\ &+\gamma\left\{\frac{\Delta\tau}{\Delta x}\left[H_y(j+1/2,k,n-1/2) - H_x(j-1/2,k,n-1/2)\right]\right. \\ &\left.-\frac{\Delta\tau}{\Delta y}\left[H_x(j,k+1/2,n-1/2) - H_x(j,k-1/2,n-1/2)\right]\right\} \end{aligned} \tag{2.18}$$

where $\beta = \left[(\varepsilon/\varepsilon_0)\sqrt{\varepsilon_0/\mu_0} - \sigma\Delta\tau/2\right] / \left[(\varepsilon/\varepsilon_0)\sqrt{\varepsilon_0/\mu_0} + \sigma\Delta\tau/2\right]$ and $\gamma = \left[(\varepsilon/\varepsilon_0)\sqrt{\varepsilon_0/\mu_0} + \sigma\Delta\tau/2\right]^{-1}$.

The stability of this scheme is easily tested by algebraically propagating a typical mode of the form $\xi^n \exp\left[-i(2\pi/\lambda)(jp_x\Delta x + kp_y\Delta y + n\Delta\tau)\right]$, where p_x and p_y represent direction cosines of this mode. [This is known as Von Neumann analysis.] It turns out that, when the condition

$$\left(\frac{\Delta\tau}{\Delta x}\right)^2 \sin^2\left(\frac{\pi p_x \Delta x}{\lambda}\right) + \left(\frac{\Delta\tau}{\Delta y}\right)^2 \sin^2\left(\frac{\pi p_y \Delta y}{\lambda}\right) \le \frac{1}{\sqrt{\beta}} \tag{2.19}$$

is satisfied, and

$$\mathrm{Re}\, n > \mathrm{Im}\, n, \tag{2.20}$$

then $0 < \beta \le 1$ and the mode amplitude is $|\xi| = \sqrt{\beta} \le 1$, so that the scheme is stable, as asserted above. If these conditions are not satisfied, then the scheme is unstable. Eq. (2.19) might seem to be a generalization of the Courant condition in Eq. (2.15), but because the direction cosines are unknown and can take on any value, and we typically have at least one non-lossy material present in our model, this condition simply reduces to the latter condition. Eq. (2.20) has been previously derived by Wong and Neureuther[16]; this result severely impacts the types of lossy media that can be simulated with the FDTD algorithm in the present form.

2.4. Radiating Boundary Conditions

Eqs. (2.16)-(2.18) provide for the simulation of the governing differential equations for the scattered fields as well as the boundary conditions in the neighborhood of each interface. [Those boundary conditions are a

Downloaded From: http://proceedings.spiedigitallibrary.org/ on 06/02/2014 Terms of Use: http://spiedl.org/terms

consequence of considering Maxwell's equations near the interface, a job naturally done by the discrete equations.] The main difficulty comes from the edge of the grid, where purely outgoing waves need to be simulated. In principle, the simplest way to proceed would be to fix the spatial component of the field at the grid to take values asserted by the asymptotic expansion in Eq. (2.14). For a general-purpose field solver, however, evaluating the necessary coefficients for each mask is not an option at present.

The simplest method of imposing these radiating boundary conditions at the edge of the grid is to use approximate absorbing boundary conditions[17]. At the edge of the grid, far from any conducting media, the field (electric or magnetic) satisfies the wave equation:

$$\left[\frac{\partial^2}{\partial x^2}+\frac{\partial^2}{\partial y^2}-\frac{\varepsilon}{\varepsilon_0}\frac{\partial^2}{\partial \tau^2}\right]E(x,y,\tau)=0. \tag{2.21}$$

The operator acting on the field can be "factored" in such a way as to stress the fact that the wave equation gives rise to both incoming and outgoing waves:

$$\left[\frac{\partial}{\partial y}+\sqrt{\frac{\varepsilon}{\varepsilon_0}\frac{\partial^2}{\partial \tau^2}-\frac{\partial^2}{\partial x^2}}\right]\left[\frac{\partial}{\partial y}-\sqrt{\frac{\varepsilon}{\varepsilon_0}\frac{\partial^2}{\partial \tau^2}-\frac{\partial^2}{\partial x^2}}\right]E(x,y,\tau)=0. \tag{2.22}$$

[The factoring was done this way because, in most cases here, we are considering the grid edge normal to $\hat{y}$.] At the edge $y=Y$, it is desired that all scattered waves with components in the $-\hat{y}$ direction be absorbed. In this case, defining $E\equiv E^{(i)}+E^{(s)}$, where the (i) denotes incident field and the (s) scattered field, the absorbing boundary condition at this edge would become

$$\left[\frac{\partial}{\partial y}+\sqrt{\frac{\varepsilon}{\varepsilon_0}}\frac{\partial}{\partial \tau}\sqrt{1-s^2}\right]\left[E^{(s)}(x,y,\tau)\right]_{y=Y}=0, \tag{2.23}$$

where $s\equiv(\partial/\partial x)/(\partial/\partial\tau)$. The operator acting on the field here is known as "pseudo-differential", and cannot be represented by any finite analog.

The best that can be hoped for is an approximation to this operator that will result in as little reflection into the grid as possible. Such an approximation is made by replacing the radical by some rational function. The quantity s can be treated as "small" compared to unity [which is plausible in light of the Courant condition], and the following approximation is made:

$$\sqrt{1-s^2}\approx\frac{\sum_{m=0}^{M}p_{2m}s^{2m}}{1+\sum_{n=1}^{N}q_{2n}s^{2n}}. \tag{2.24}$$

Good results have been shown for the case of this rational function corresponding to the $[2M,2N]$ Pade approximant of the radical[18]. [That is, the first $2M+2N+1$ terms in the Taylor series of both sides of Eq. (2.6) are identical.] Furthermore, it has been shown that a necessary and sufficient condition for stability is[19] $N\in\{M-1,M,M+1\}$.

Downloaded From: http://proceedings.spiedigitallibrary.org/ on 06/02/2014 Terms of Use: http://spiedl.org/terms

The simplest case corresponds to $[2M,2N]=[0,0]$; here, the boundary condition becomes $\left[(\partial/\partial y)-\sqrt{\varepsilon/\varepsilon_0}(\partial/\partial\tau)\right]\left[E^{(s)}(x,y,\tau)\right]_{y=Y}=0$. If one propagates a plane wave given by $E^{(s)}(x,y,\tau)=\exp\left[-i2\pi(x\sin\vartheta+y\cos\vartheta+\tau)/\lambda\right]$ to this boundary, then the reflected amplitude here is $-(1-\cos\vartheta)/(1+\cos\vartheta)$, which is zero only in air at normal incidence. Because the mask is usually embedded in a dielectric such as quartz, this reflection coefficient will take on larger values and the error involved in this zeroth-order approximation will be unacceptable. It turns out that the case $[2M,2N]=[2,0]$ provides a reasonable amount of absorption at the boundary. The boundary condition for E-polarization here, upon using Eq. (2.7), is simplified to

$$\left[\frac{\partial}{\partial y}+\sqrt{\frac{\varepsilon}{\varepsilon_0}}\frac{\partial}{\partial\tau}\right]\left[E_z^{(s)}(x,y,\tau)\right]_{y=Y}-\frac{1}{2}\frac{\sqrt{\mu_0\varepsilon}}{\varepsilon_0}\left[\frac{\partial}{\partial x}H_y^{(s)}(x,y,\tau)\right]_{y=Y}=0. \quad (2.25)$$

One can show that the reflected amplitude is now $-\left[(1-\cos\vartheta)/(1+\cos\vartheta)\right]^2$, so that the reflection error is reduced drastically[20]. In principle, one can continue to reduce this reflection error by going to higher orders, but this second-order approximation is sufficient for the purposes of this paper.

The absorbing boundary conditions act only on the scattered portion of the field; nevertheless, it is the total field that is propagated. One way to deal with this is to simply subtract the incident field [which is known analytically] from the total field in the vicinity of the boundaries, apply the boundary condition, and then add back the incident field. A more efficient means of applying these conditions to the total field, however, that is less susceptible to roundoff error is possible. To illustrate, note that the typical incident field in our simulations is a normally incident plane wave in air. The equation satisfied by this field is

$$\frac{\partial E_z^{(i)}}{\partial y}-\frac{\partial E_z^{(i)}}{\partial\tau}=0, \quad (2.26)$$

and this equation is to be added to Eq. (2.25). Because $H_y^{(i)}=0$ for normal incidence, the boundary condition for the total field can be expressed in terms of the known initial field. A similar analysis occurs for the other edge.

There are two final notes: first, discretizing Eq. (2.25) is similar to that for Maxwell's equations, but stability is ensured if one averages over the fixed coordinates. Second, there are rational approximations to the radical other than that in Eq. (2.24) which may prove to be more convenient (in terms of using higher-order approximations to the radical) in a user-friendly software package than what is used here, and such approximations are the subject of current research[21].

2.5. Comparison with exact results

The best way to test the finite-differencing algorithm is to have a nontrivial case available in which an analytical solution exists. The following examples are simple cases designed to provide a verification of the correctness of the algorithm outlined above.

Downloaded From: http://proceedings.spiedigitallibrary.org/ on 06/02/2014 Terms of Use: http://spiedl.org/terms

2.5.1. Layered Medium

Consider a plane wave in air (index = n_1), normally incident on a thin film at $y = 0$ of index of refraction n_2 and thickness D, and this thin film has been deposited onto a substrate of index n_3. The electric field within the thin film has been shown to take the form[22]

$$E(x,y) = 2n_1 \frac{(n_2+n_3)\exp[ik_2(D-y)] + (n_2-n_3)\exp[-ik_2(D-y)]}{(n_1+n_2)(n_2+n_3)\exp[ik_2 D] + (n_1-n_2)(n_2-n_3)\exp[-ik_2 D]} E^{(i)}(x), \tag{2.27}$$

where $k_2 = 2\pi n_2 / \lambda$. Upon taking the values for the indices of refraction $n_1 = 1, n_2 = 2, n_3 = 4$ and setting $\lambda = 500\text{nm}$ and $D = 1000\text{nm}$, the value of the field amplitude throughout the region surrounding the film becomes

$$|E(y)| = \begin{cases} 0.4, & y < -D \\ 0.4\sqrt{1+3\sin^2(4\pi y/\lambda)}, & -D < y < 0 \\ 0.4\sqrt{1+15\sin^2(2\pi y/\lambda)}, & y > 0. \end{cases} \tag{2.28}$$

The results of the FDTD calculation are in Fig. 1, and it is clear that the errors involved here are very small.

2.5.2. Sommerfeld Half-plane

The simplest and best-known case of an exact result in rigorous diffraction theory is that for an infinitely thin, perfectly-conducting half-plane, whose exact solution was discovered by Sommerfeld in 1896. Let the conductor be in the plane $y = 0,\ x > 0$, and consider a plane wave incident from the half-space $y > 0$. If the function $g(s) = \exp[-is^2]\operatorname{erfc}[s\exp(-i\pi/4)]$, then the total field is given by[23]

$$E_z(x,y,\tau) = \frac{1}{2}\exp\left[i\frac{2\pi}{\lambda}(r-\tau)\right]\left\{g\left[-\sqrt{\frac{4\pi}{\lambda}}r\cos\left(\frac{\vartheta-\alpha_0}{2}\right)\right] - g\left[-\sqrt{\frac{4\pi}{\lambda}}r\cos\left(\frac{\vartheta+\alpha_0}{2}\right)\right]\right\}, \tag{2.29}$$

where $x = r\cos\vartheta$, $y = r\sin\vartheta$, and α_0 is the angle the incident wave makes with the surface of the conductor. [For a normally incident plane wave, $\alpha_0 = \pi/2$.]

The results of both the exact and the FDTD calculations are presented in Fig. 2. An important feature of this computation is that these results were obtained by propagating the scattered component of the field rather than the total field itself. That is, Eq. (2.18) is modified in the regions outside of free space to include a source term, rather than including the source term in the boundary conditions. (This is not necessary for the other equations, as the materials are not magnetic.) A comparison with this computation performed by propagating scattered and total fields showed that, for this computation (and only this computation from all those in this paper), given exactly the same grid spacing, etc., the scattered field computation had far less error. The reason behind this is not clear yet, but a rule of thumb of when to use total vs. scattered field formulations is one subject of current research.

Downloaded From: http://proceedings.spiedigitallibrary.org/ on 06/02/2014 Terms of Use: http://spiedl.org/terms

3. Integration with PROLITH/2

The output of a typical mask topography simulation described above will take the form of a 1D "transmittance" of the mask, i.e., the amplitude and phase of the electric field directly beneath the bottom of the mask. By considering this transmittance to be an arbitrary 1D gray-scale mask, it is easily integrated into the PROLITH/2 simulation environment. The complex transmission function to be input into PROLITH/2 is sampled at the plane immediately below the feature with the largest depth. With coherent illumination, PROLITH/2 easily computes the diffracted orders and a comparison of any results using this new transmission function against the corresponding Kirchhoff mask is readily available.

The real potential challenge lies with partially coherent illumination. In general, the mask transmission function will depend on the angle of incidence of the illumination. As each simulation is a very expensive (i.e., long) computation, the possibility of performing several such computations at various angles for a single mask simulation becomes less than desirable. The Hopkins approximation, which states that the only effect of an oblique angle of incidence is the shifting of the diffraction pattern[24], provides relief by removing this angular dependence from the transmission function. Furthermore, Wong[25] has shown that this approximation is good when the angle of incidence is less than 30°. Therefore, we need to compute only the normally incident case for most applications.

The following examples represent standard cases that will illustrate when the Kirchhoff approximation becomes invalid. A rule-of-thumb is that when the smallest feature is about a wavelength, one must use a full electromagnetic computation to get reasonable accuracy. Although this assumption is the subject of active research, it will be interesting to see how much error there is in the aerial images in the cases that follow. In all of the examples below, the systems are illuminated by a conventional DUV source (248 nm) with a partial coherence factor of 0.5 and a numerical aperture of 0.6. The mask is made up of chrome-like elements of index $2.5 + i\,2.0$ that have a depth of 100 nm and are set on glass of index 1.51. The goal in all cases is to print a 0.25 μm line.

3.1. *Isolated Line*

In printing a single line, it is natural to simulate the effect of a single element on the aerial image. In order to print a subwavelength line, a stepper with a magnification of, say, 4X is employed. Within the Kirchhoff approximation, the only difference in the aerial image between the line imaged with the 4X stepper and a line 4 times as small imaged with a 1X stepper is in the radiometric factor in the inner integral in Eq. (1.1)[26]

$$K(f_x) = \left(\frac{1 - \lambda^2 f_x^2 / R^2}{1 - \lambda^2 f_x^2} \right)^{1/4}, \tag{3.1}$$

where R is the reduction factor (4 in the case above). As this factor is typically close to unity [For the parameters given above, the average value of this function over the NA range is about 1.03.], one would not expect much variation between 4X and 1X imaging.

In Fig. 3, the results of the FDTD computation are presented for the case of 4X reduction. The field in the vicinity of the mask is presented in (a) and (b), and it is clear that there is an obvious departure from the Kirchhoff field here. The most prominent features of these plots are the smoothing out of the discontinuities introduced by the Kirchhoff approximation, and the ringing of the amplitude along a transverse plane. The amplitude of this ringing decreases with the distance from the nearest chrome feature. The phase of the field below the mask is not presented as there is a negligible departure from what is introduced by Kirchhoff. In (c), the aerial image is computed, and this is compared to the corresponding image using the standard Kirchhoff approximation, as calculated using PROLITH/2. Note that the only appreciable difference between these two images is at the first maximum of the intensity.

Downloaded From: http://proceedings.spiedigitallibrary.org/ on 06/02/2014 Terms of Use: http://spiedl.org/terms

The results of using the same mask, but with 1X magnification, are shown in Fig. 4. Note that the difference in the aerial image from the Kirchhoff approximation is much greater, as one might expect. The prediction here is that the image width is somewhat larger than one would expect if a rigorous computation had not been considered.

3.2. *Equal Lines and Spaces*

The next example to consider is a mask made up of equal lines and spaces. This problem can be looked at in one of two ways: as scattering by the chrome, or diffraction by an aperture in the chrome. The results for the 4X case are shown in Fig. 5, and the 1X in Fig. 6. Note that, in Fig 5(b), the intensity in each space has 4 maxima, while in Fig 6(b), it has 1 maxima. This is a general trend that is repeatedly confirmed throughout the rest of the paper: for a space N waves wide, there will be N maxima in the mask transmittance function. In both cases, there does not seem to be more than a 2% difference in the aerial image intensities between the full EM case and the Kirchhoff case.

3.3. *Alternating Phase-Shifting Mask*

We also considered imaging a 0.25 μm line using an alternating phase-shifting mask. This mask is similar to that considered by Wojcik, *et al*[7], except that we use DUV illumination and magnifications of 4X and 1X. The results of this computation are shown in Figs. 7 and 8, respectively. For the 4X case, the phase deviates little from the constant phase-shift expected, and the aerial image intensity shows the characteristic features noted by prior computations: a decrease in peak intensity in the lobe corresponding to the phase-shifted region, and a slight narrowing of the linewidth (in contrast to that found for the isolated line). For the 1X case, however, the results are much more drastic. The mask transmission function seems to have the beginnings of some nontrivial phase variation, and the peak intensity directly under the phase shift has been reduced severely. The result is an aerial image that is radically different from the corresponding Kirchhoff approximation. In fact, the peak intensity of the phase-shifted region has changed so much that the Kirchhoff model will fail to make even crude qualitative predictions about which features will print.

3.4. *Proximity-Correcting Scattering Bars*

Finally, we considered the case of a 0.25 μm chrome line surrounded by 0.0625 μm scattering bars placed 0.3125 μm from the edges of the line (1X dimensions). Note that there are indeed 5 maxima in each space between the line and the scattering bars for this 4X mask. The importance of this example, however, lies in the difference between the rigorous and Kirchhoff models. The purpose of the scattering bars is to reduce the difference between isolated and a dense line by making the isolated line "look" dense. Of course, it is imperative that the side dips caused by the scattering bars are shallow enough that they do not print. The rigorous model shows us that, in this case, the Kirchhoff model underestimates the printability of these scattering bars.

4. Conclusions

We have shown that, for some cases, rigorous electromagnetic modeling is crucial in predicting lithographic phenomena accurately. While it is clear that such rigorous modeling is necessary in most cases when the smallest feature is a wavelength or smaller, it can also be important when that feature size is somewhat larger, especially in phase-shifting masks.

Future work will take on a few different directions. One such direction will be towards improving the FDTD model in terms of efficiency and stability. One of the main focuses of this effort will be deriving a scheme that is stable, even when the conditions in Eq. (2.20) are violated. Another direction this research effort will take is in finding ways to model the electromagnetic effects without relying on an expensive algorithm like FDTD. The

Downloaded From: http://proceedings.spiedigitallibrary.org/ on 06/02/2014 Terms of Use: http://spiedl.org/terms

goal in finding such an algorithm is to find a correction that has a computation time on the order of that for Kirchhoff. The ultimate result of this effort will take the form of a fast, accurate, and robust electromagnetic simulator, coupled with a full lithography model, to more accurately simulate the lithographic effects of mask topography.

References and Notes

[1] C. Mack, *Inside PROLITH*, Austin: FINLE Technologies, Inc., 1997, Ch.2 B & C.
[2] Interesting discussions of diffraction problems for which the Kirchhoff approximation represents an exact solution can be found in F. Kottler, "Diffraction at a black screen", *Progress in Optics*, vol. IV, pp. 281-314 (1966), and E.W. Marchand & E. Wolf, "Consistent Formulation of Kirchhoff's Diffraction Theory", *J. Opt. Soc. Am.* **56**, 1712-1722 (1966).
[3] G.W. Forbes, D.J. Butler, R.L. Gordon, A.A. Asatryan, "Algebraic corrections for paraxial wave fields", *J. Opt. Soc. A,. A* **14**, 3300-3315 (1997).
[4] C. Yuan, "Calculation of One-Dimensional Lithographic Aerial Images Using the Vector Theory", *IEEE Trans. Electron Devices* **40**, 1604-1613 (1993).
[5] A.K. Wong & A.R. Neureuther, "Mask Topography Effects in Projection Printing of Phase-Shifting Masks", *IEEE Trans. Electron Devices* **41**, 895-902 (1994).
[6] C. Pierrat, A. Wong, S. Vaidya, M. Vernon, "Phase-Shifting Mask Topography Effects on Lithographic Image Quality", *SPIE Vol. 1927*, 28-41 (1993).
[7] G. Wojcik, J. Mould, Jr., R. Ferguson, R. Martino, K.K. Low, "Some image modeling issues for I-line, 5x phase shifting masks", *SPIE Vol. 1927,* 455-465 (1994).
[8] R.A. Ferguson, A.K. Wong, T.A. Brunner, L.W. Liebmann, :Pattern-Dependent Correction of Mask Topography Effects for Alternating Phase-Shifting Masks", *SPIE Vol. 1927*, 349-360 (1995).
[9] V.D. Barger & M.G. Olsson, *Classical Electricity and Magnetism*, Boston: Allyn and Bacon, Inc., 1987, p. 381.
[10] M. Born & E. Wolf, *Principles of Optics*, Oxford: Pergamon Press, 1980, p. 52.
[11] See, for example, T.B.A. Senior & J.L. Volakis, *Approximate boundary conditions in electromagnetics*, London: The Institution of Electrical Engineers, 1995.
[12] B.B. Baker & E.T. Copson, *The* Mathematical *Theory of Huygen's Principle,* Oxford: Clarendon Pres, 1950, Ch. 1, Secs. 5-6.
[13] S.N. Karp, "A convergent far-field expansion for the two-dimensional radiation functions", *Commun. Pure Appl. Math.* **14**, 427-434 (1961).
[14] K.S. Yee, "Numerical Solution of initial boundary value problems involving Maxwell's equations in isotropic media", *IEEE Trans. Ant. Prop.*, **14**, 302-307 (1966).
[15] W.H. Press, S.A. Teukolsky, W.T. Vetterling, & B.P. Flannery, *Numerical Recipes in C*, Cambridge: Cambridge University Press, 1992, Sec. 19.1. They go on to show that, with this so-called "staggered leapfrog" type of scheme, for the 1D wave equation, there is also no amplitude dissipation suffered. The proof for the 2D case here is a simple extension.
[16] A.K. Wong, A.R. Neurether, "Rigorous Three-Dimensional Time-Domain Finite-Difference Electromagnetic Simulation for Photolithographic Applications", *IEEE Trans. Semiconductor Manufacturing* **8**, 419-431 (1995).
[17] There are many works in the literature dealing with this topic. The first to suggest a pseudo-differential operator approach [and an approximation with a rational function] appears to be E.L. Lindman, "'Free-Space' Boundary Conditions for the Time-Dependent Wave Equation"" *J. Comp. Phys.* **18**, 66-78 (1975). The most cited work on these boundary conditions is B. Engquist and A. Madja, "Absorbing boundary conditions for the numerical simulation of waves", *Math. Comp.* **31**, 629-651 (1977). The first paper geared toward the solution of Maxwell's equation rather than the wave equation was G. Mur, "Absorbing Boundary Conditions for the Finite-Difference Approximation of the Time-Domain Electromagnetic Field Equations", *IEE Trans. Elec. Comp.* **EMC-23**, 377-382 (1981). Eq. (2.25) can be derived using analysis from this latter paper.
[18] P.A. Tirkas, C.A. Balanis, R.A. Renaut, "Higher Order Absorbing Boundary Conditions for the Finite-Difference Time-Domain Method", *IEEE Trans. Ant. Prop.* **40**, 1215-1222 (1992).
[19] L.N. Trefethen, L. Halpern, "Well-Posedness of One-Way Wave Equations and Absorbing Boundary Conditions", *Math. Comp.* **47**, 421-435 (1986).

Downloaded From: http://proceedings.spiedigitallibrary.org/ on 06/02/2014 Terms of Use: http://spiedl.org/terms

[20] A good measure of the amplitude error δ is a weighted average of the reflection coefficient $R(\vartheta)$ over all possible angles: $\delta = \int_{-\pi/2}^{\pi/2} d\vartheta\, R(\vartheta) \cos\vartheta \,/\, \int_{-\pi/2}^{\pi/2} d\vartheta \cos\vartheta$. For the zeroth-order boundary condition, $\delta = \pi - 3 \approx 0.142$, while for that in Eq. (2.28), $\delta = 19/3 - 2\pi \approx 0.050$.

[21] For an implementation of such a method, see Ref. 18. The analysis performed in this work is greatly simplified using a result from K. McInturff and P.S. Simon, "Closed-Form Expressions for Coefficients Used in FD-TD High-Order Boundary Conditions", *IEEE Microwave and Guided Letters* **3**, 222-223 (1993).
[22] C.A. Mack, "Analytical expression for the standing wave intensity in photoresist", *Appl. Opt.* **25**, 1958-1961 (1986).
[23] This form of Sommerfeld's solution can be found in Ref. 10, pp. 569-570.
[24] See H.H. Hopkins, "The concept of partial coherence in optics", *Proc. Royal. Soc.*, **A208**, 263-277 (1951). Note that this approximation here takes the form of the assumption that the point spread function of an optical system only depends on the difference of the coordinates in the object and image planes. This is also presented in great detail in Born & Wolf, pp. 526-532.
[25] Alfred K. Wong, "Rigorous Three-Dimensional Time-Domain Finite-Difference Electromagnetic Simulation", Ph.D. Thesis, Memorandum No. UCB/ERL M94/69, U. Cal., Berkeley (1994). The question of how many samples over σ-space are actually needed to produce a certain accuracy is addressed in detail in Robert J. Socha, "Propagation Effects of Partially Coherent Light in Optical Lithography and Inspection", Ph.D. Thesis, Memorandum No. UCB/ERL M97/55, U. Cal., Berkeley (1997).
[26] *Inside PROLITH*, p. 33.

Downloaded From: http://proceedings.spiedigitallibrary.org/ on 06/02/2014 Terms of Use: http://spiedl.org/terms

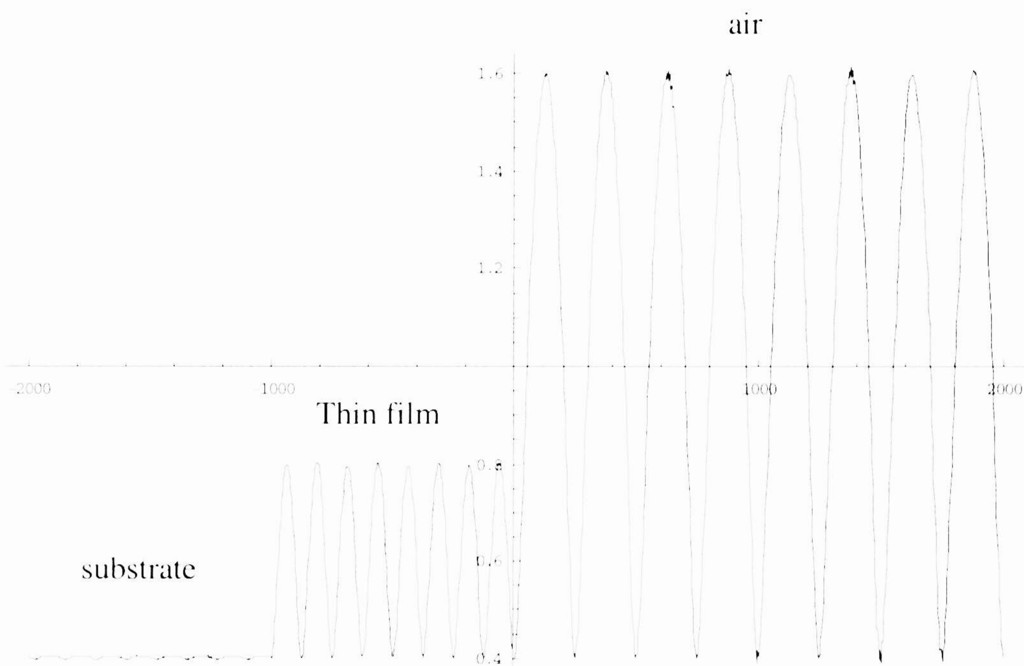

Fig. 1. FDTD computation of field amplitude in the vicinity of the thin film; compare to Eq. (2.28).

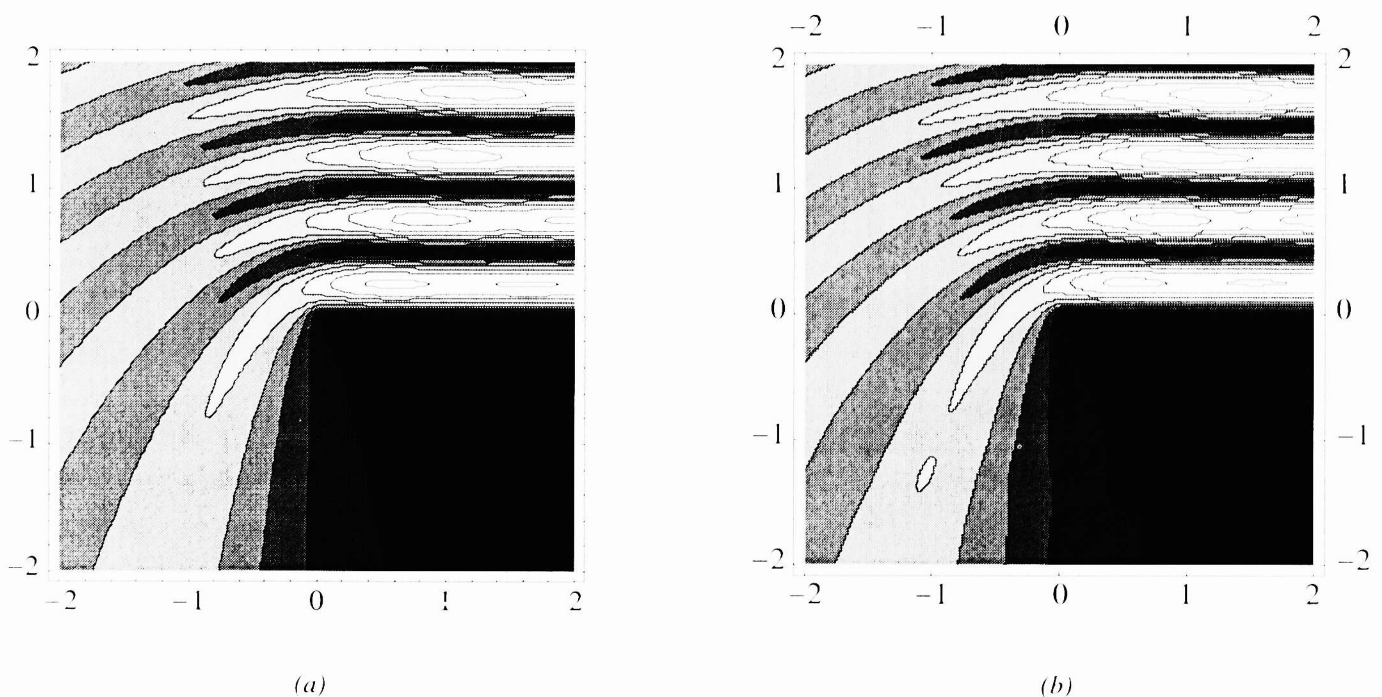

Fig. 2. (a) Exact field amplitude of an E-polarized electric field in the neighborhood of an infinitely thin, perfectly-conducting half-plane. (b) The same computed with the FDTD algorithm. The x & y-axes are in units of wavelengths.

Downloaded From: http://proceedings.spiedigitallibrary.org/ on 06/02/2014 Terms of Use: http://spiedl.org/terms

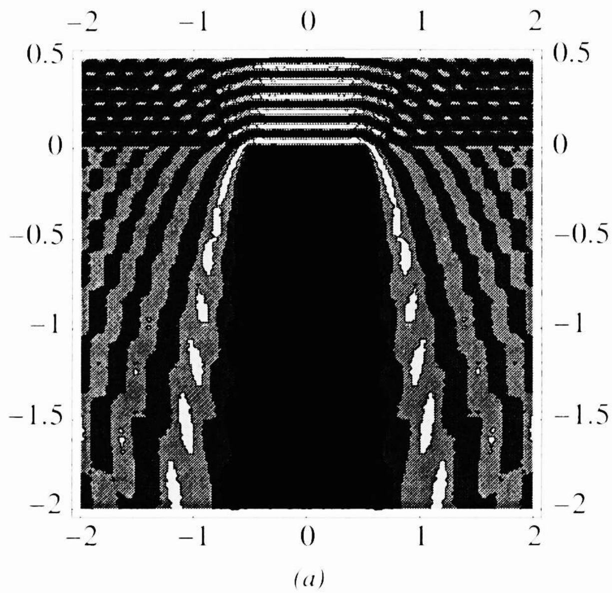

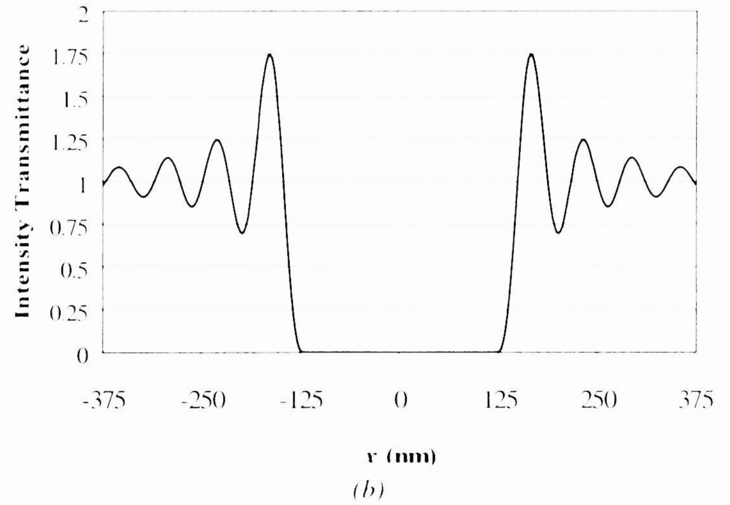

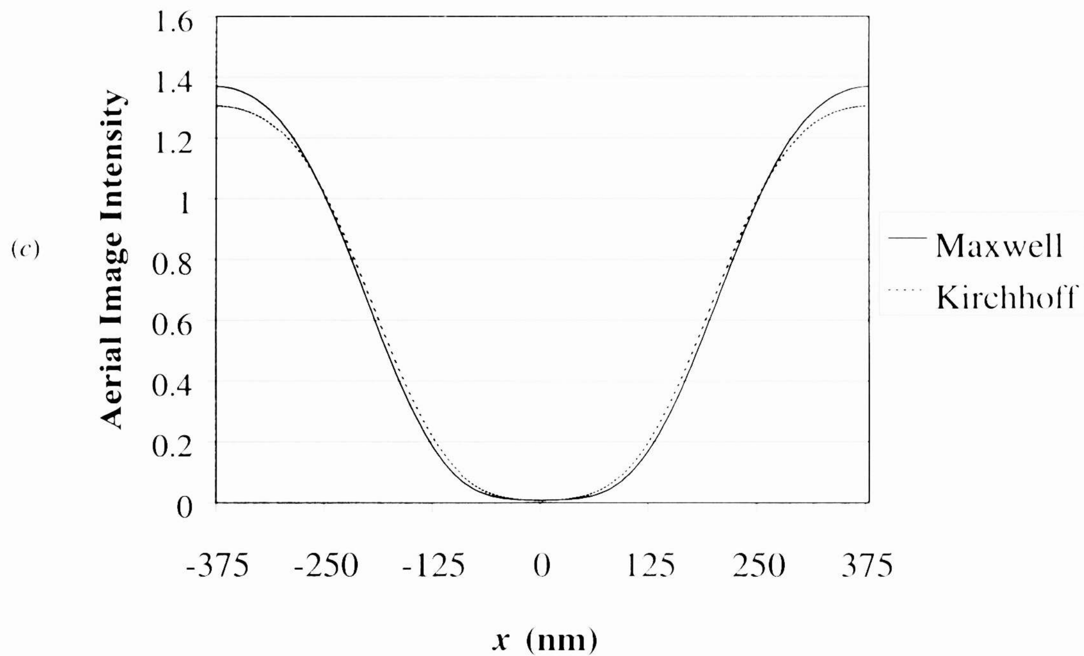

Fig. 3. (a) The electric field intensity in the vicinity of a 4X, 0.25 μm chrome line. Note that the axes are in mask dimensions and are in microns. (b) The field intensity immediately below the chrome. The ordinate is scaled in wafer coordinates and are in nm. (c) The aerial image intensity due to the transmission function of the mask and its counterpart due to the Kirchhoff approximation.

Downloaded From: http://proceedings.spiedigitallibrary.org/ on 06/02/2014 Terms of Use: http://spiedl.org/terms

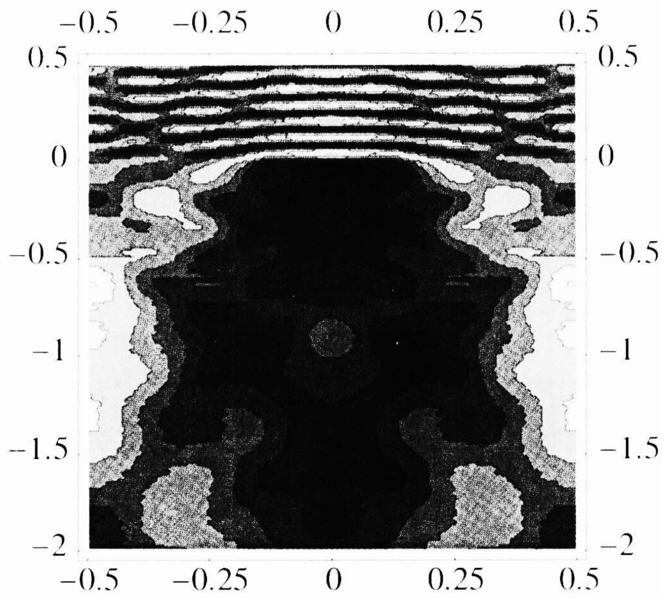

(a)

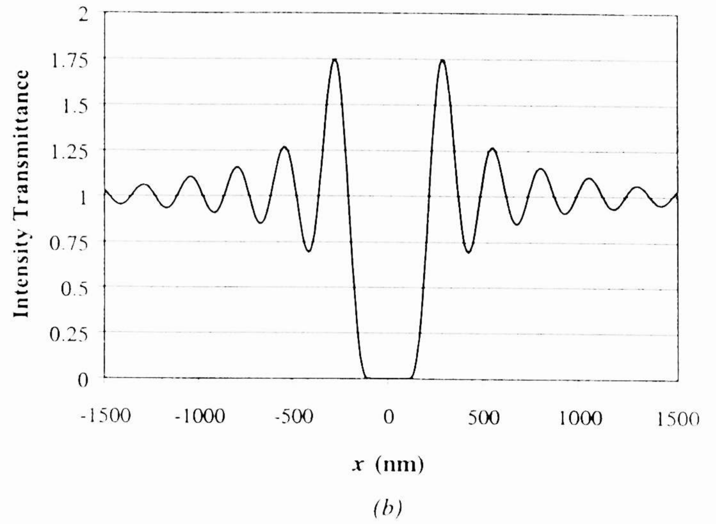

(b)

(c)

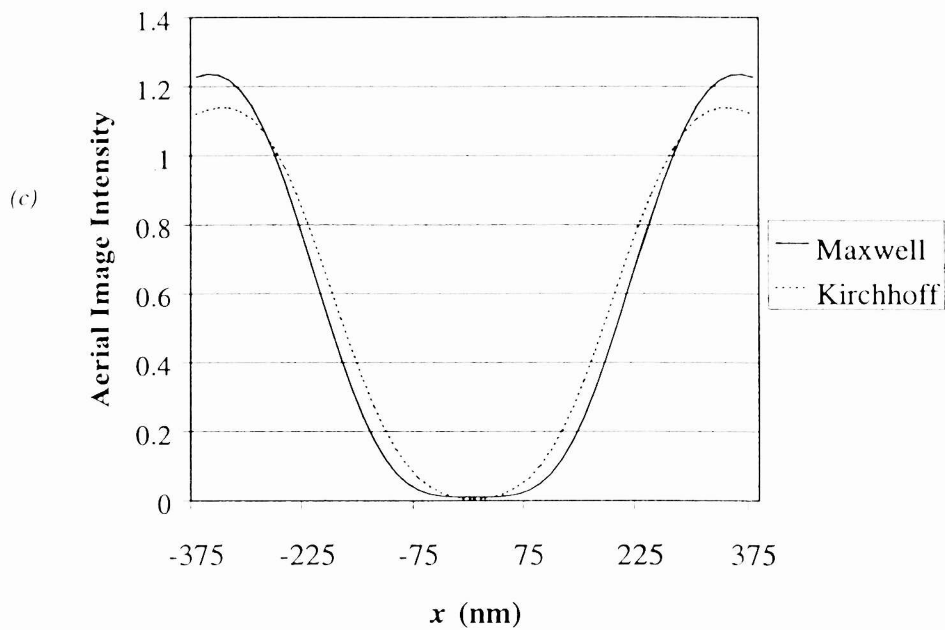

Fig. 4. Same as Fig. 3, except for a 1X chrome line.

Downloaded From: http://proceedings.spiedigitallibrary.org/ on 06/02/2014 Terms of Use: http://spiedl.org/terms

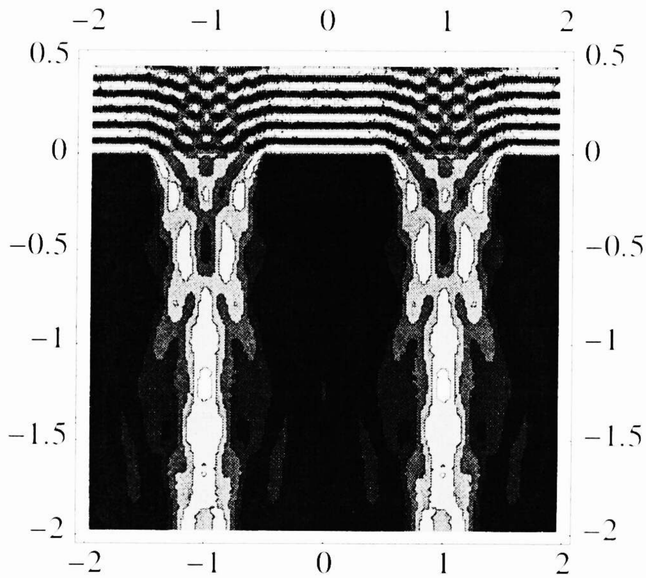

(a)

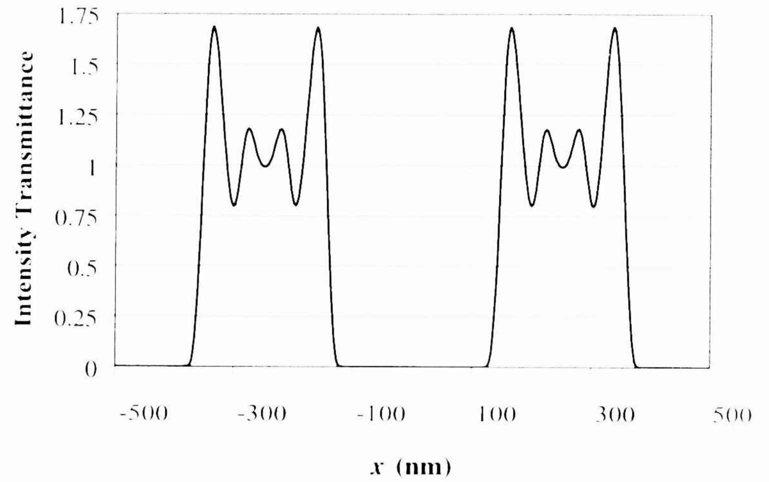

(b)

(c)

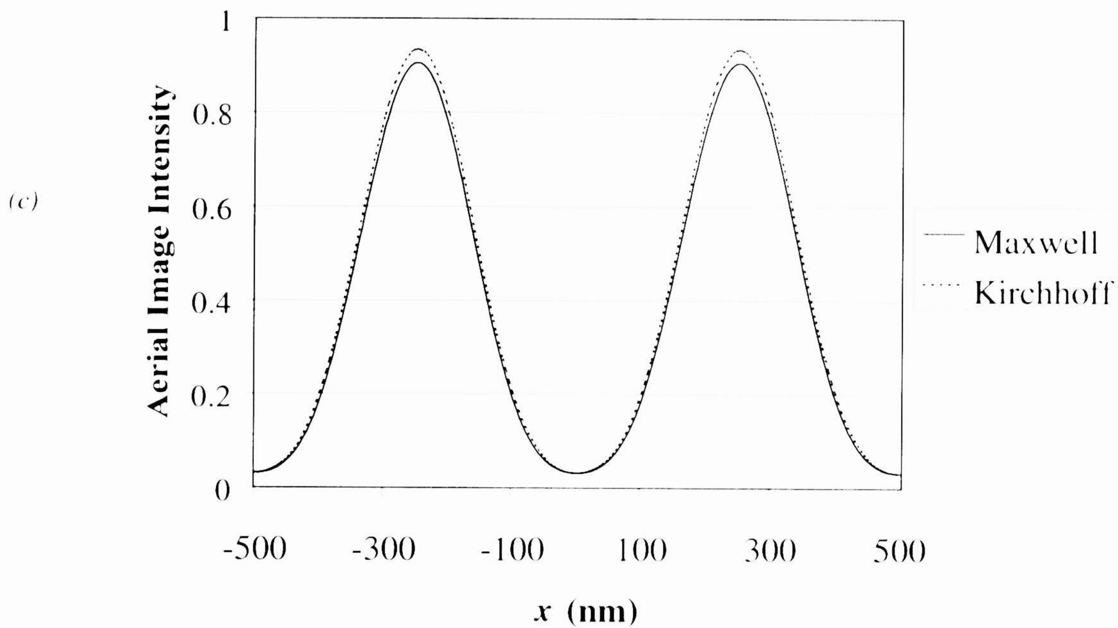

Fig. 5. Same as Fig. 3, but for 0.25 μm equal lines and spaces, 4X reduction.

Downloaded From: http://proceedings.spiedigitallibrary.org/ on 06/02/2014 Terms of Use: http://spiedl.org/terms

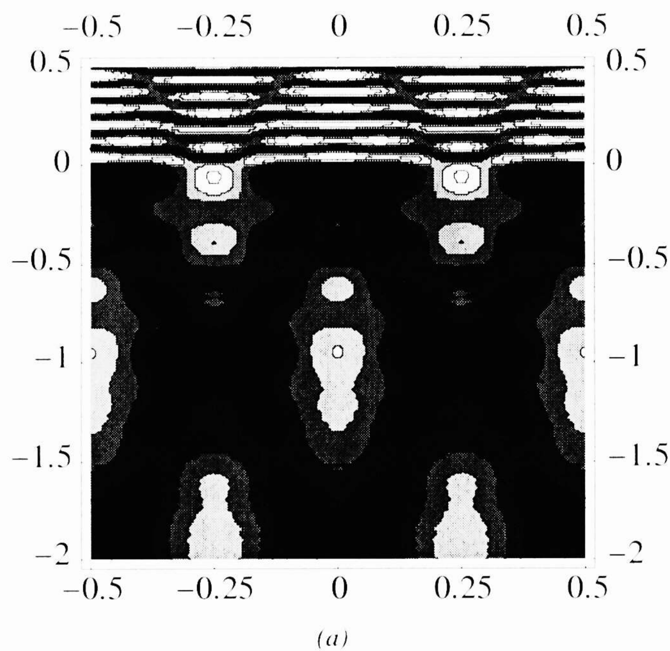

(a)

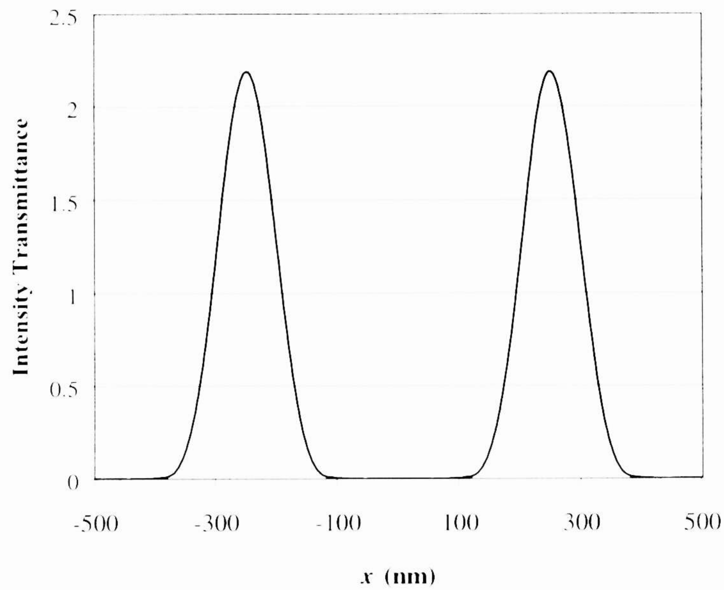

(b)

(c)

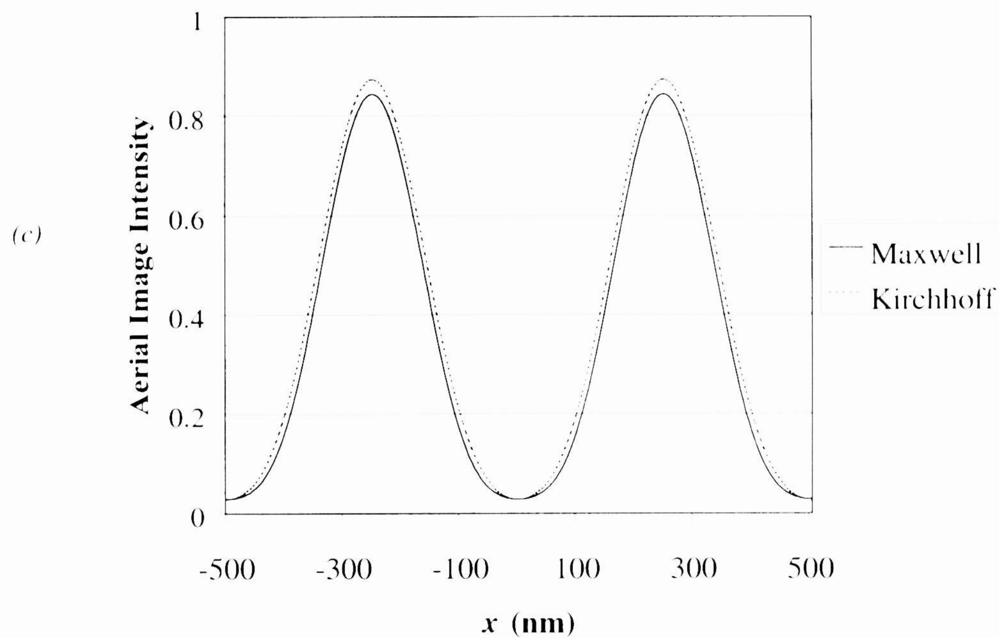

Fig. 6. Same as Fig. 5, except for a 1X magnification.

Downloaded From: http://proceedings.spiedigitallibrary.org/ on 06/02/2014 Terms of Use: http://spiedl.org/terms

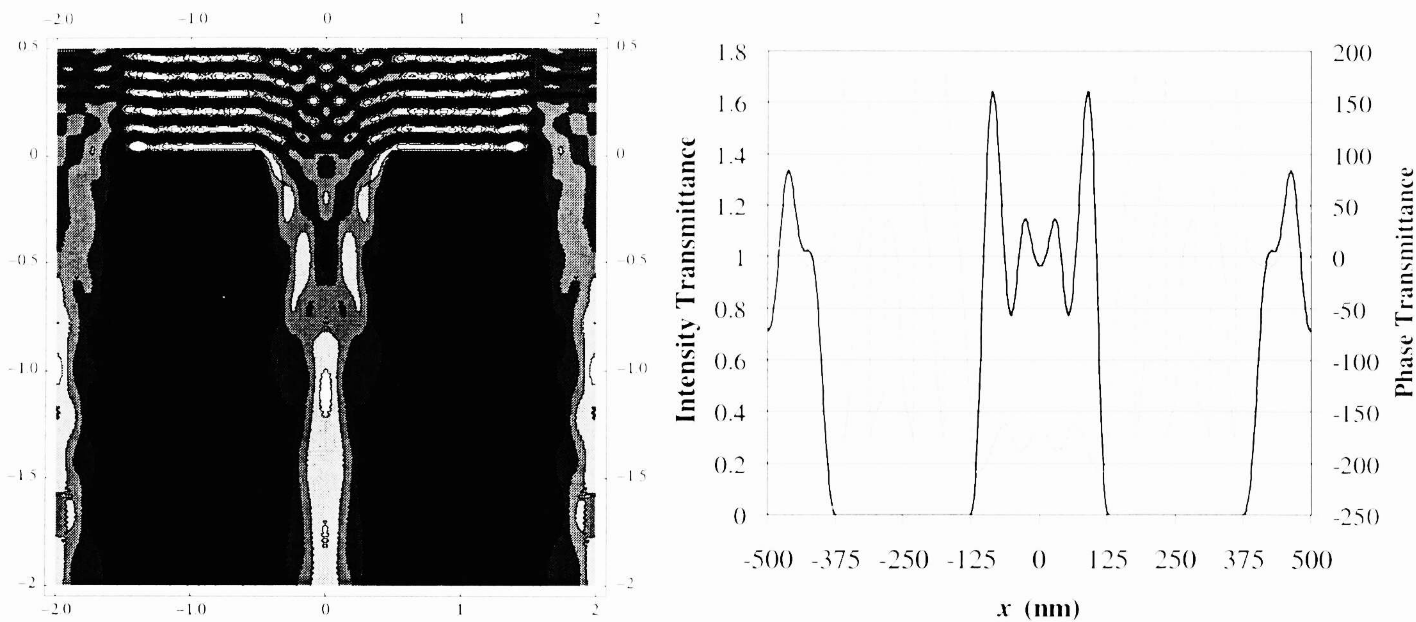

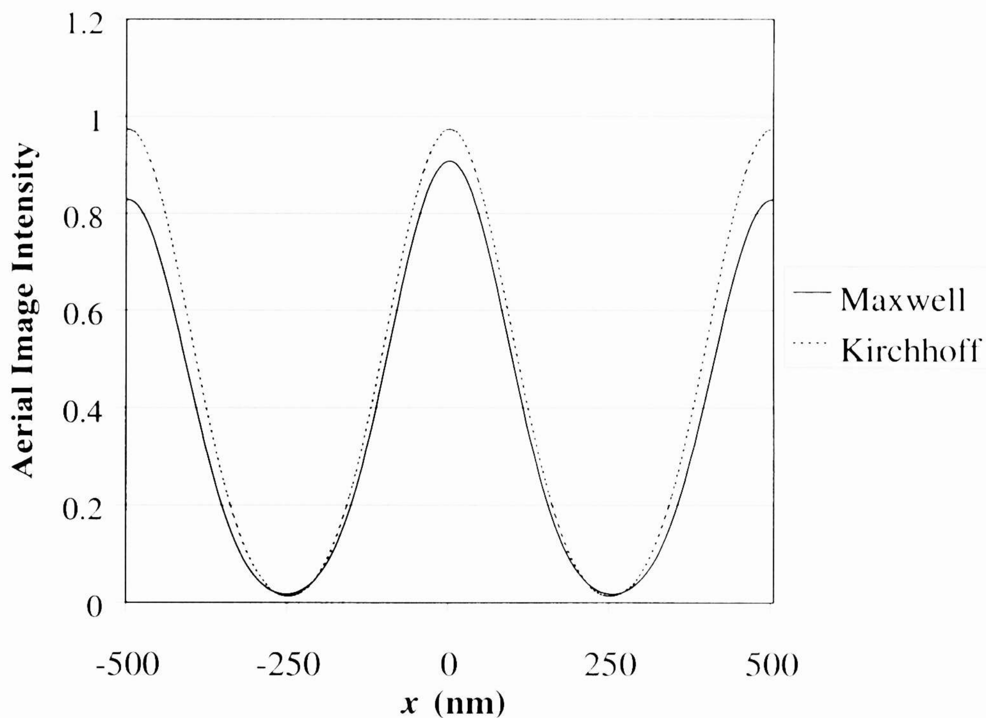

Fig. 7. Same as Fig. 3, except for an alternating (Levenson) 0.25 μm, 4X phase-shifting mask. Phase-shifted spaces are made subtractively, with the glass substrate removed to the appropriate depth to give a nominal 180° phase shift, and with no undercutting of the chrome. In this case, the center space is not shifted.

Downloaded From: http://proceedings.spiedigitallibrary.org/ on 06/02/2014 Terms of Use: http://spiedl.org/terms

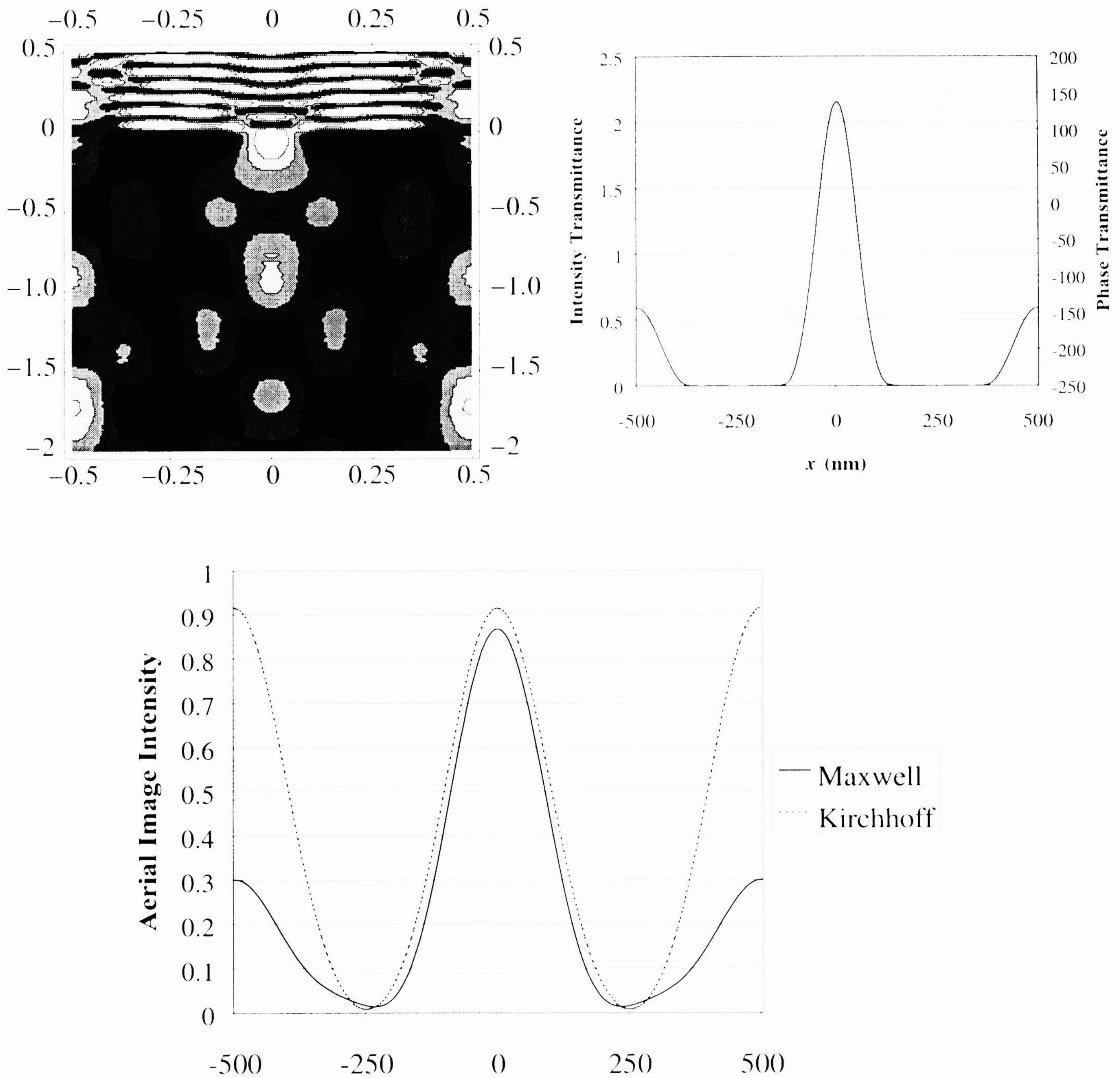

Fig. 8. Same as Fig. 7, except for a 1X magnification.

Downloaded From: http://proceedings.spiedigitallibrary.org/ on 06/02/2014 Terms of Use: http://spiedl.org/terms

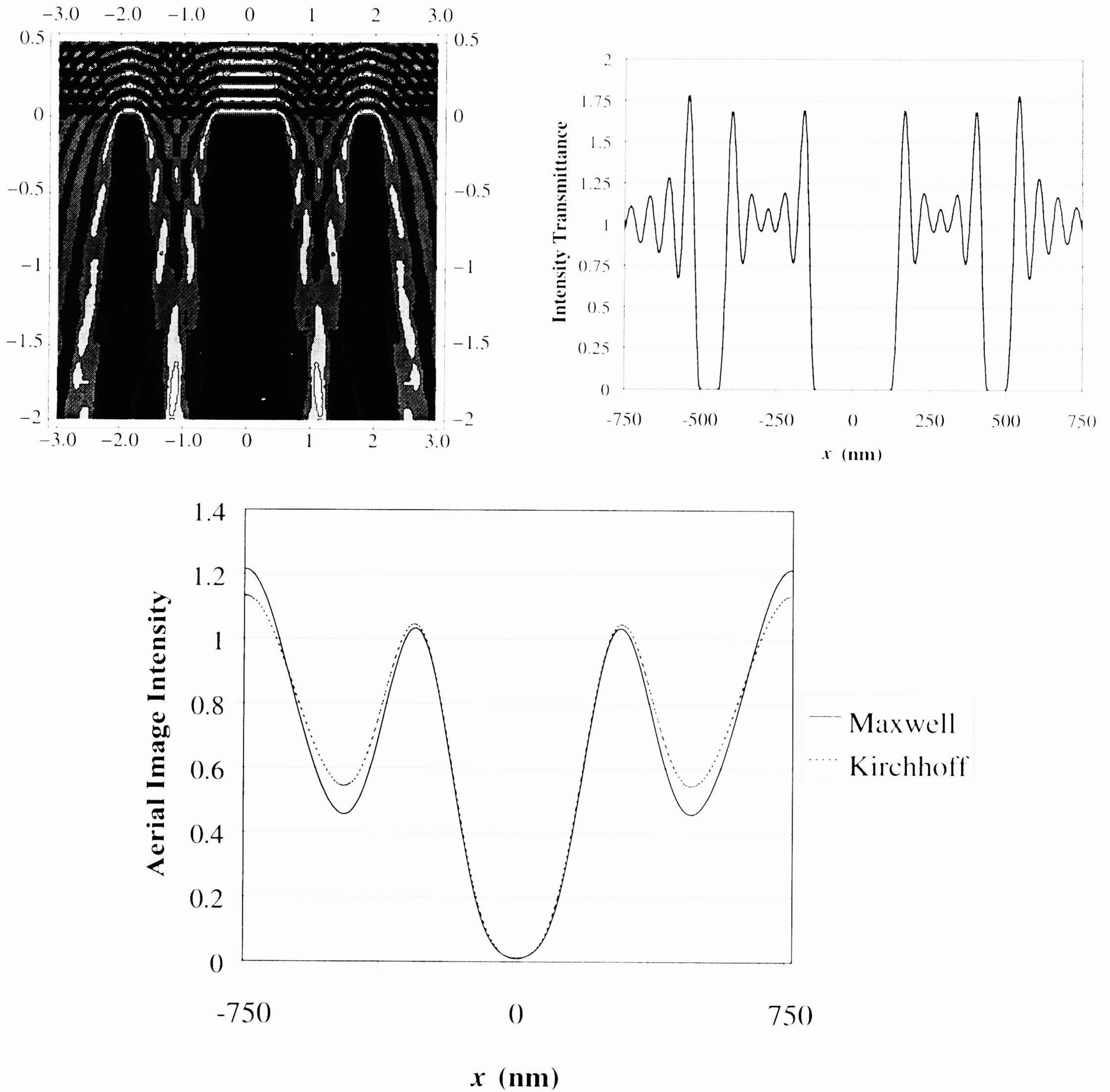

Fig. 9. Same as Fig. 3, except for a 0.25 μm chrome line with 0.0625 μm scatter bars placed 0.3125 μm from each end of the line.

Downloaded From: http://proceedings.spiedigitallibrary.org/ on 06/02/2014 Terms of Use: http://spiedl.org/terms